JOURNAL OF MATERIALS SCIENCE **36** (2001) 5719–5728

Porous Ni/TiO_2 substrates for planar solid oxide fuel cell applications

F. MESCHKE*, F. J. DIAS, F. TIETZ‡
Forschungszentrum Jülich, Institut für Werkstoffe und Verfahren der Energietechnik (IWV), D-52425 Jülich, Germany
E-mail: f.tietz@fz-juelich.de

Anode substrates based on Ni/TiO_2 cermets were fabricated for planar solid oxide fuel cells (SOFCs) with the aim of reducing the material costs and preventing thermoelastic bending of the currently used Ni/8YSZ-based cells. Ni/TiO_2 substrates were produced via sintering of NiO/$NiTiO_3$ powder compacts and subsequent reduction. The sintering behavior in air and the resulting microstructure were studied in detail. Excellent electrical conductivity and gas permeability was achieved before and after reduction due to coarse microstructure. The co-firing behavior of substrates coated with an anode layer and an 8YSZ electrolyte membrane was analyzed with the aim of identifying those sintering schedules which give flat cells with a gastight electrolyte. Thermoelastic bending of cells is negligible since the thermal expansion coefficient is well adjusted to the 8YSZ electrolyte.

1. Introduction

Reducing the operating temperature of solid oxide fuel cells (SOFCs) to below 800°C is currently a main topic in SOFC development, because at these temperatures limited oxidation rates allow the use of commercial ferritic steels [1]. With the reduction of electrolyte thickness and the minimization of the ohmic resistance of the membrane, Forschungszentrum Jülich (FZJ) has made considerable progress in lowering the application temperature while maintaining the electrical performance. The FZJ fuel cell design is based on a 1.5 mm thick anode cermet of Ni/8YSZ as the substrate coated with a thin 8YSZ electrolyte, on top of which a cathode layer is deposited [2, 3]. By reducing the electrolyte thickness to 15 μm [1] it is possible to operate the SOFC at 750°C with a power output level only delivered by electrolyte-supported cells with an electrolyte thickness of about 200 μm at a 200–250°C higher temperature [4].

Further improvement to cell performance was also achieved by optimizing the anode and cathode layers [1, 5]. The anode has basically three tasks, namely current pickup, the supply of mechanical strength to the cell and the electrocatalytic conversion of the fuel. This is currently realized by a double layer system based on Ni/8YSZ and composed of an anode substrate and a so-called 'anode functional layer' for the electrochemical conversion of the fuel [1, 6]. Cell performance was improved by optimizing the structure of the anode functional layer [1]. The substrate also still has potential for improvement with respect to the thermal expansion coefficient (TEC), gas permeability and material costs. New cermets based on cheap oxides like Al_2O_3 or TiO_2 have been synthesized as substrate materials in a previous study [7]. With a TEC matching 8YSZ, these substrates reduce the costs of the cells and avoid thermoelastic bending during cell fabrication [8] and thermal cycling. The present study especially deals with the sintering behavior, resulting microstructure and the physical properties of NiO/$NiTiO_3$ substrates. Major attention is focused on the co-firing behavior and the resulting interface microstructure when coated with a NiO/8YSZ-based anode layer and an 8YSZ electrolyte. These coated substrates are hereafter referred to as **s**ubstrate-**a**node-**e**lectrolyte assemblies (SAE assemblies). The principal aim is to identify optimized co-firing conditions of SAE assemblies in terms of physical properties, microstructure, curvature and electrochemical performance. A key tool is the *in situ* observation of the bending behavior during co-firing and during temperature changes with a long-distance microscope [9]. Results of a preliminary cell test are presented and discussed in terms of the specific assembly microstructure.

2. Experimental

2.1. Material composition

The TEC of the substrates can be tailored to that of 8YSZ by adjusting the ratio of volume fractions of NiO and $NiTiO_3$ in the substrate. An appropriate composition was selected by the following consideration. According to the formula proposed by Thomas [10], the

*Now with Elektroschmelzwerk Kempten GmbH, Germany.
‡Author to whom all correspondence should be addressed.

0022–2461

TEC of a multiphase composite with volume fractions >15% of each phase is determined by

$$\alpha = \prod_i \alpha_i^{v_i} \quad (1)$$

with α_i representing the mean TEC for the temperature interval $\Delta T = 30$–1000°C and v_i being the volume fraction of phase i. The theoretically obtained TEC values of the NiO-$NiTiO_3$-TiO_2 system are shown in Fig. 1 as a function of the molar fraction of NiO. In Fig. 2 the data are plotted for the Ni-TiO_2 system versus the volume fraction of Ni. In the NiO-$NiTiO_3$-TiO_2 system the TEC increases slowly in the NiO-poor region, because the TEC of $NiTiO_3$ ($\alpha = 10.4 \times 10^{-6}\,K^{-1}$) is somewhat higher than that of TiO_2 ($\alpha = 9.1 \times 10^{-6}\,K^{-1}$) [11]. A good agreement with the TEC of the solid electrolyte 8YSZ ($\alpha = 10.6{-}11.1 \times 10^{-6}\,K^{-1}$) [12, 13] was found for compositions containing 55–65 mol% NiO yielding a cermet composition with 40 vol% Ni after reduction. Consequently, a starting composition of this regime was chosen.

2.2. Processing of components

Starting materials for the preparation of porous anode substrates [7, 14] were NiO (>99%, J. T. Baker) and TiO_2 (Bayertitan® PK 5594, 99.7%, Bayer). The $NiTiO_3$ starting powder was obtained by mixing an equimolar amount of NiO and TiO_2 and calcining it at 1200°C to form the binary oxide $NiTiO_3$. The reaction product was ball milled and NiO was added to adjust the predetermined ratio of NiO/$NiTiO_3$. The chosen starting composition of the substrate with a nickel content of 40 vol% after reduction enabled a direct comparison with the standard YSZ-based substrate [1]. Applying the coat-mix process [7, 14–16] for powder preparation, a NiO/$NiTiO_3$ powder with agglomerate sizes between 20 and 100 μm was obtained. Green substrates were obtained by uniaxial die pressing at about 130°C under a pressure of 1 MPa. The substrates were 2 mm thick and had a surface area of 70×70 mm^2 [7, 15].

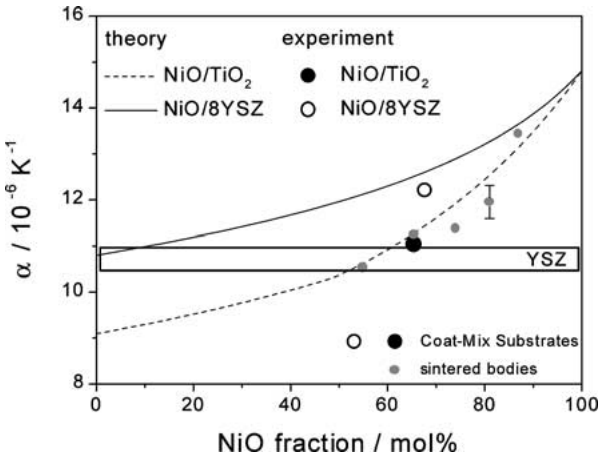

Figure 1 Calculated and experimental TECs of NiO/8YSZ and NiO/TiO_2 composites. The formation of $NiTiO_3$ is considered and the reason for the different slopes of the calculated TEC curve for NiO/TiO_2 below and above 50 mol% NiO.

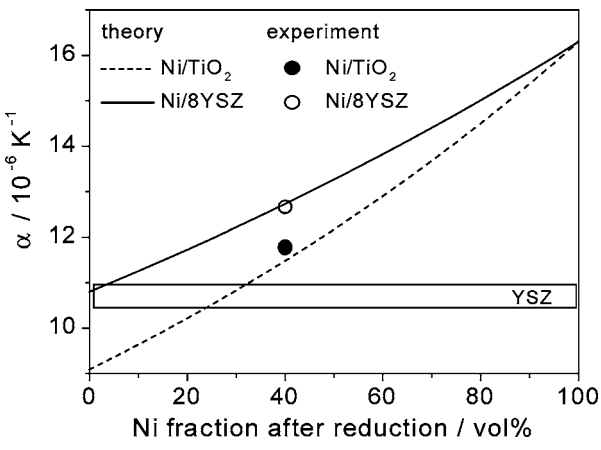

Figure 2 Calculated and experimental TECs of Ni/8YSZ and Ni/TiO_2 cermets.

For the sintering and gas permeability experiments disks of 25 mm in diameter were prepared. After calcining at 800°C in a chamber furnace the sintering temperature was increased by 100°C at a rate of 1 K/min and the dimensional changes were subsequently measured. This procedure was repeated up to 1400°C and then isothermal sintering was carried out for 20 h at intervals of 5 h.

Quadratic cells with dimensions of 50×50 mm^2 were manufactured for electrochemical tests starting with pre-sintering of green substrates at 1100°C for 3 h. An anode functional layer composed of NiO and 8YSZ (50 wt% each) and an 8YSZ solid electrolyte layer was applied onto the highly porous plates by vacuum-assisted slip casting [3, 17]. Co-firing was carried out at 1300°C for 5 h. The anode and the electrolyte layer then had a thickness of 5 μm and 15 μm, respectively. Finally, a 60 μm thick, double-layered cathode was applied onto the electrolyte by wet powder spraying. The first and electrocatalytically active layer consisted of 40 wt% 8YSZ and 60 wt% $La_{0.65}Sr_{0.3}MnO_3$ and the second layer was pure $La_{0.65}Sr_{0.3}MnO_3$ [5]. Finally, these SAE assemblies complete with cathodes were sintered at 1200°C for 5 h.

For *in situ* co-firing experiments some of the green SAE assemblies were cut into rectangular specimen (8×35 mm^2). With one of their wide front sides being polished to a 1 μm finish their bending behavior was analyzed with a long-distance microscope (see also 2.3.2).

2.3. Characterization techniques

2.3.1. Physical substrate properties

Thermal expansion measurements were carried out on 25-mm-long substrate specimens in a horizontal push-rod dilatometer (Netzsch DIL 402C) between room temperature and 1100°C. The dilatometer was calibrated with sapphire single crystal and Ni-20Cr alloy (VA-Chromium) [18]. The electrical conductivity of the resulting cermets was measured after reduction in Ar/4% H_2 at 900°C for 2 h by a 4-probe DC technique in the temperature range of 30–900°C. Silver paste and silver wires were used as contacts and wrapped around the rectangular samples cut from substrate plates to dimensions of approx. $30 \times 5 \times 2$ mm^3. Gas permeability measurements were performed as described in [15] on disks with a diameter of about 20 mm after sintering. For differential thermal analysis and thermogravimetry

a simultaneous thermal analyzer (Netzsch STA 409C) was used.

2.3.2. Co-firing behavior of SAE assemblies

The co-firing behavior of green SAE assemblies was studied *in situ* with a long-distance microscope (Questar QM100). Using this microscope, contour changes of the specimens could be observed at high temperature through a window port in the furnace. Attention was focused especially on bending behavior during heating and during isothermal hold at the sintering temperature. In order to quantify the deflection, a semicircle was fitted to the specimen contour and a radius of curvature, R, was determined. Due to the limited diameter of the window port, the contour of the specimen could only be determined on a profile 24 mm in length. The center deflection was calculated for a virtual specimen length of $L = 100$ mm from the estimated radius of curvature by

$$\delta = R \cdot \left(1 - \cos\left(\frac{L}{2 \cdot R}\right)\right) \qquad (2)$$

The specimens were heated at a rate of 3 K/min to temperatures of 1280°C to 1350°C including a binder burn-out step at 350°C for 1 h. The dwell times at the sintering temperature varied between 0.5 and 4 h. The specimens were cooled to room temperature at a rate of 8 K/min.

2.3.3. Thermoelastic bending behavior

In order to evaluate the thermoelastic bending behavior of free moveable SAE assemblies caused by temperature changes, a long-distance microscope was used to observe specimens with dimensions of $35 \times 10 \times 1.5$ mm^3 which were placed un-clamped on a plane sample holder made of alumina. The specimens were heated to a maximum temperature of 900°C in a Ar/4% H_2 gas atmosphere. Those with a substrate sintered at 1400°C were used as SAE assemblies. Induced by the temperature change, the specimens could freely bend according to the differences in TEC. The Ar/4% H_2 gas atmosphere causes a reduction of the initially oxidized substrate and enables the bending behavior of oxidized and reduced substrates to be evaluated in a single experiment. Because the reduction kinetics are slow at temperatures below 700°C [19], the thermoelastic bending of the oxidized NiO/$NiTiO_3$ substrate was determined over a sufficient temperature range during heating. At temperatures higher than 700°C NiO is reduced to Ni and bending due to the reduction (mainly from the loss of mechanical strength accompanying the reduction of NiO to Ni, see Chapter 3.6) is superposed on the thermoelastic effect. Once reduction is completed, the thermoelastic bending of the SAE assembly with a reduced substrate was monitored during cooling. Heating and cooling was performed with a ramp of 3 K/min, the holding time at 900°C was 30 min.

2.4. Electrochemical test

For a preliminary evaluation of electrochemical performance, a NiO/$NiTiO_3$ SAE assembly co-fired at 1350°C was selected for examination. The specimen was coated with a lanthanum manganite cathode as described in section 2.2. While the fuel cell size was 50×50 mm^2, the cathode effective area was 45×45 mm^2. The border of uncoated electrolyte was used as space for a gold sealing. A platinum and a nickel mesh were used as electrical contacts on the cathode and anode side, respectively, in a ceramic housing. Hydrogen (1000 ml/min humidified with 1.4% H_2O) and air (1000 ml/min) were used as the fuel and oxidant, respectively. Fuel utilization was 2.3%, while air utilization was 5.8%. Current-voltage curves in the temperature range between 650 and 900°C were measured at the beginning and after operation for one week at 800°C by applying a constant load of 0.15 A/cm^2.

3. Results and Discussion

3.1. Substrate sintering behavior

The sintering behavior of NiO/$NiTiO_3$ substrates is compared to conventional NiO/8YSZ in Fig. 3. During heating to 1400°C the NiO/$NiTiO_3$ substrate densified considerably faster than NiO/8YSZ. For example, at 1300°C the standard substrate shrank by 10% while the TiO_2-based substrate revealed a shrinkage of 19%. After reaching the final sintering temperature of 1400°C both substrates continued to densify substantially during the following 5 h. Thereafter shrinkage is low. The overall shrinkage is approx. 31% in the case of NiO/$NiTiO_3$ and about 23% for NiO/8YSZ.

Compared with conventional NiO/8YSZ, the sintering kinetics of NiO/$NiTiO_3$ was significantly enhanced as shown in Fig. 3. By plotting the shrinkage data in an Arrhenius-type diagram an activation energy of sintering of 387 kJ/mol and 233 kJ/mol was calculated for NiO/8YSZ and NiO/$NiTiO_3$, respectively [14]. The lower activation energy is the reason for the improved densification behavior of the NiO/$NiTiO_3$ substrates. In addition, with increasing sintering temperature the microstructure coarsened considerably, leading to TiO_2 grain sizes in the range of 5–20 μm (Fig. 4) although

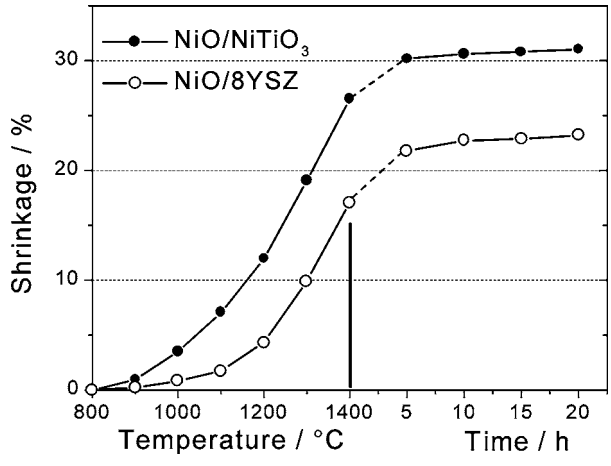

Figure 3 Shrinkage curves for a NiO/$NiTiO_3$ substrate and a NiO/8YSZ substrate currently used in SOFC development. The NiO/$NiTiO_3$ densifies much faster at lower sintering temperatures. No significant differences are obtained for isothermal sintering at 1400°C (right-hand side of the figure).

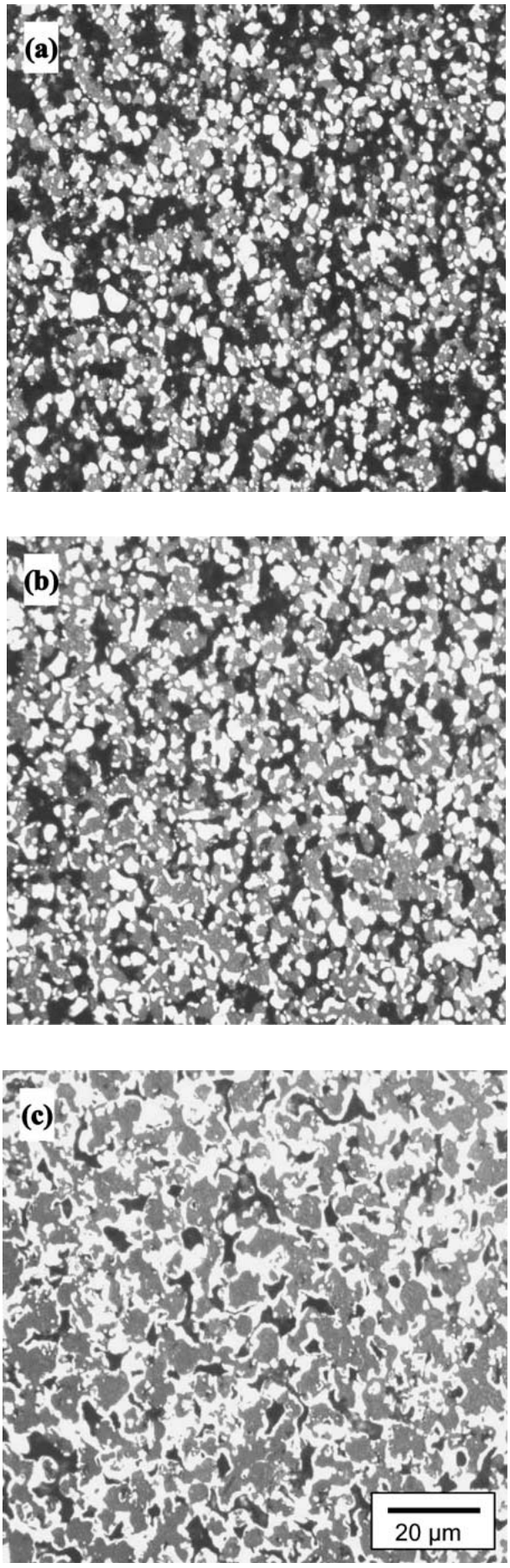

Figure 4 Microstructure of Ni/TiO_2 cermet substrates after sintering in air for 5 h and subsequent reduction at 900°C (2 h), (a) sintered at 1200°C, (b) sintered at 1300°C and (c) sintered at 1400°C. Black: pores, gray: ceramic phase, white: Ni.

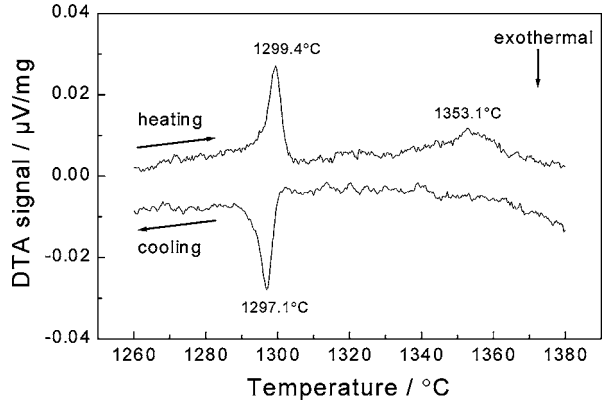

Figure 5 High temperature part of the DTA curves showing the DTA signals during heating and cooling of a $NiO/NiTiO_3$ substrate specimen. Both the heating and cooling rate was 3 K/min.

the initial particle sizes of the starting powders was in the 1–3 μm range. This strong grain coarsening in combination with round-edged grain morphology suggests a liquid phase sintering process. Differential thermal analysis in air showed a small but very narrow endothermic and exothermic peak during heating and cooling, respectively, at 1298 (±2)°C (Fig. 5). Also a broader peak around 1350°C was observed during heating. Apparently a partial melting (and solidification during cooling) occurs at 1298°C, which might be related to the dissolution of Ni and Ti in zirconia [14]. Although $NiTiO_3$ can dissolve significant amounts of NiO [20], this should not decisively lower the melting point of the composite. Instead, a transmission electron microscopy (TEM/EDX analysis) study revealed small droplet-like particles with a mean diameter of 250 nm at the grain boundaries [14] containing high amounts of Ni and Ti, but also Zr and small amounts of Y. The presence of Zr and Y indicate that wear debris of the milling media (yttria partially stabilized zirconia, Y-PSZ) was incorporated as impurities into the substrate powder. These elements might have the potential to lower the melting point of $NiO/NiTiO_3$ so that a liquid phase was formed at 1300°C.

3.2. Substrate microstructure

The microstructure of substrates sintered either at 1200°C, 1300°C or 1400°C for a fixed dwell time of 5 h are shown after reduction at 900°C for 2 h in Ar/4% H_2 in Fig. 4. The reduction was performed only to distinguish the different solid phases very clearly. Although the reduction changes the pore structure, because Ni has a smaller unit cell volume than NiO, the influence of reduction with respect to the wetting of TiO_2 by Ni metal can be regarded as small. The NiO particles admixed to $NiTiO_3$ during powder fabrication transformed to nickel during reduction and were distributed homogeneously around TiO_2 grains after reduction. The metal phase, the ceramic phase and the porosity, all covering roughly the same volume fraction, form interpenetrating networks. With increasing sintering temperature the porosity decreased from 52% at 1200°C to 33% at 1400°C.

After sintering at 1200°C the microstructure consists of coarse nickel grains (3–10 μm) and numerous

sub-micron nickel particles which appear white or light gray in Fig. 4a. The TiO_2 grains (dark gray) have a mean diameter of about 2–3 μm.

Sintering at 1300°C gave a coarser microstructure as evidenced by Fig. 4b. The amount of sub-micron nickel particles in the TiO_2 grains is reduced significantly and a Ni film starts to cover the TiO_2 grains. Apart from the fact that zirconia has been replaced by titania, the described microstructure is very similar to Ni/8YSZ cermets of SOFC anodes in particular with respect to grain size and porosity.

Sintering at 1400°C leads to further grain coarsening and TiO_2 grains now appear round-edged (Fig. 4c). In this case all sub-micron nickel particles seem to have vanished and instead a continuous nickel network has developed. Nickel oxide started to form a continuous layer on titania grains, which we relate to the partial melting process as mentioned earlier. The TiO_2 grains coarsened to a diameter of 5–15 μm.

A common feature found in all specimens is that the titania grains exhibit intragranular precipitates of nickel after reduction. This specialty is due to the decomposition of $NiTiO_3$ to NiO and TiO_2 during the reduction process and a simultaneous transformation of NiO to Ni. The size of the precipitates can be controlled by the reduction temperature.

3.3. Physical properties of substrate

3.3.1. Thermal expansion coefficient

The measured α-values of $NiO/NiTiO_3$ and NiO/8YSZ substrates agree quite well with the theoretical values as shown in Fig. 1. Also the TECs of the reduced Ni/TiO_2 cermet substrate coincide with the theoretical value (see Fig. 2). From the figures it also becomes clear that the TECs of both the oxidized and the reduced substrate can be tuned in a range between $9 \times 10^{-6}\,K^{-1}$ and $16 \times 10^{-6}\,K^{-1}$ as a function of nickel content. Consequently, the anode substrates containing TiO_2 can be adjusted to any electrolyte material currently under consideration. As an example, the regime for the TEC of 8YSZ [12, 13] is also shown in both figures.

An additional remark should be made concerning the Ni/TiO_2 cermet. The experimental value shown in Fig. 2 is an extrapolated value obtained by a polynominal fit [14], because the original expansion curve is strongly bent from about 700°C due to softening of the Ni/TiO_2 substrate. The softening is clearly an advantage in terms of stress relaxation when stresses are built up within assembled stacks. However, knowledge concerning long-term mechanical stability is still missing.

3.3.2. Electrical conductivity and gas permeability

The results of the conductivity and gas permeability measurements are presented in Fig. 6 as a function of porosity of the cermet substrates. The different porosity was a result of using sintering temperatures of 1200, 1300 and 1400°C. Obviously, specimens for conductivity measurement and those for gas permeability exhibited differences in porosity due to the different specimen types. However, a clear interrelation of porosity, conductivity and gas permeability can be deduced. The electrical conductivity increases strongly with decreasing porosity whereas the gas permeability decreases linearly. For comparison, the corresponding value of the conventional Ni/8YSZ cermet is also shown. When the Ni/TiO_2 substrate was sintered at 1300°C, the conductivity is similar to Ni/8YSZ. In this case, however, the gas permeability of the Ni/TiO_2 is about three times higher. If the comparison is focused on similar gas permeability, the Ni/TiO_2 (sintered at 1400°C) shows about three times higher electrical conductivity at 10% lower porosity.

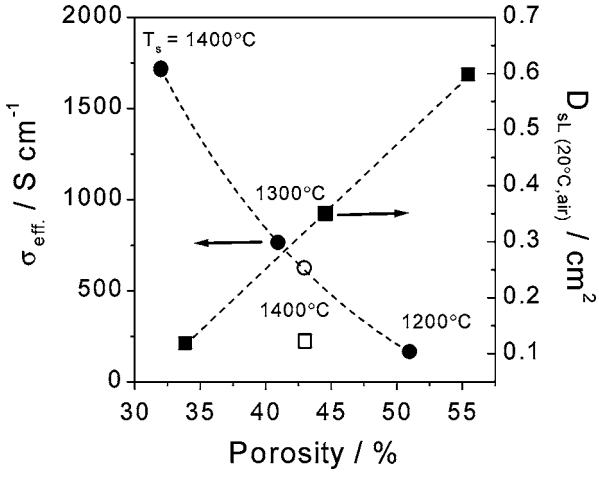

Figure 6 Electrical conductivity (σ_{eff}) at 800°C (circles) and gas permeability (D_{sL}) at 20°C in air (squares) as a function of porosity. Sintering temperatures of the samples are indicated. The open symbols indicate the values for the Ni/8YSZ cermet sintered at 1400°C.

Due to the coarse microstructure with large pores, the Ni/TiO_2 cermets exhibited three times better gas permeability at a given porosity than Ni/8YSZ cermets (Fig. 6) [7, 15]. The strong increase of electrical conductivity with sintering temperature is not only due to higher density but also to a well developed interpenetrating network of Ni, which is highly interconnecting.

3.4. Co-firing related bending of assemblies

During co-firing the initially plane $NiO/NiTiO_3$ SAE assemblies remained flat up to 1100°C. They started to bend towards the electrolyte side at a temperature of typically 1100°C and increased continuously up to 1300°C. Differences in the densification behavior of substrate and electrolyte- and anode coating are regarded as the cause of the bending. The onset temperature coincides with the temperature at which the 8YSZ coating material starts to sinter [21]. The direction of bending agrees with that of a shrinking coating.

Substantial shape changes occurred intermediately between 1280°C and 1350°C. As a measure of the curvature the central deflection of a 100 mm long specimen is given in Fig. 7. The diagram reveals that the central deflection reached a maximum value of 5.8 mm at 1300°C. Heating beyond 1300°C caused the deflection to drop to 3.8 mm at 1350°C. Similar bending behavior has been observed for NiO/8YSZ substrate-based assemblies [21]. The rapid increase in the central

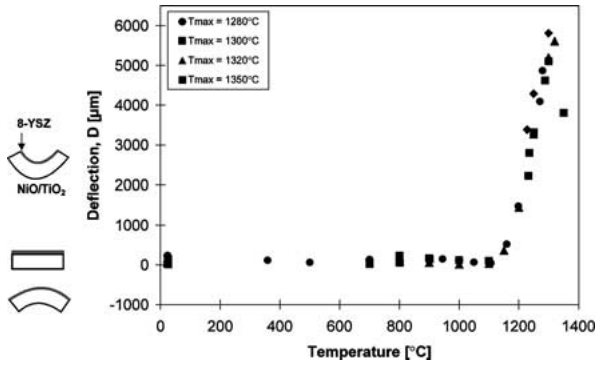

Figure 7 Bending of $NiO/NiTiO_3$ SAE assemblies during heating to maximum sintering temperatures between 1280°C and 1350°C.

deflection indicates that the coating densifies much faster than the substrate. The observed drop of the central deflection during heating to final sintering temperatures of 1320°C and 1350°C, respectively, can be explained in terms of re-sintering of the substrate and a decreasing densification rate of the coating. A decreasing densification rate is primarily due to approaching final density.

Fig. 8 exhibits the time dependence of the bending behavior during isothermal holds between 1280°C and 1350°C. The deflection diminished continuously with increasing time except during co-firing at 1280°C. In that case, bending first increased until a maximum central deflection of 5.6 mm at 30 min was reached before the deflection decreased continuously. The deflection reached values close to zero or even slightly negative values after sufficiently long exposure times. Depending on temperature, the time to reach zero deflection increased from 30 min at 1350°C to 75 min at 1320°C, 120 min at 1300°C and about 195 min at 1280°C. With decreasing temperature a longer dwell time is required in order to obtain zero central deflection due to the different kinetics effect of sintering. The sinter kinetics of both the substrate and the coating becomes slower with decreasing temperature. However, irrespective of the temperature of each sinter cycle, with an appropriate time schedule flat components can be achieved in all cases.

It is important to note that subsequent cooling to room temperature did not result in any substantial bending. The variation in central deflection during cooling was

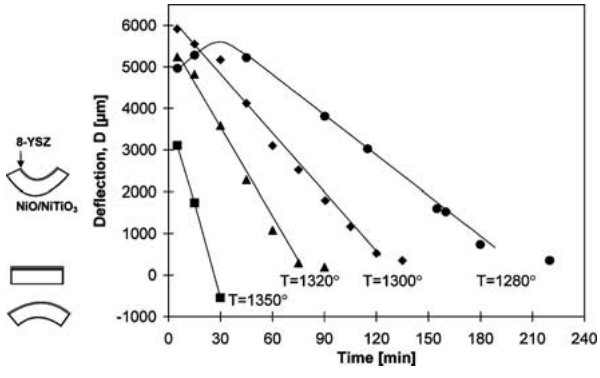

Figure 8 Bending characteristics of $NiO/NiTiO_3$ SAE assemblies during sintering at different temperatures.

smaller than the experimental scatter. This is a first indirect proof that TEC values of substrate and electrolyte had been well adjusted.

3.5. Anode and electrolyte microstructure

It is of great importance for cell performance to know the best temperature and time schedules for yielding dense electrolytes and at the same time highly electrochemical active anodes. Cross-sections of co-fired assemblies showing the substrate and the anode/electrolyte interface after reduction are presented in Fig. 9 and in Fig. 10, respectively. It is evident from Fig. 9 that the specimens which were sintered between 1280°C and 1350°C until planarity was achieved all reveal a 10-μm-thick and gastight electrolyte layer (light gray in contrast). Hence, the main requirement of dense electrolyte is met in all of the cases.

The anode was about 5 μm thick in each case as shown by Fig. 10. However, depending on sintering temperature the structure differed significantly in porosity and in grain size. Co-firing at 1280°C yielded a highly porous anode. The zirconia grains of the anode had a size similar to that of the electrolyte (0.5 μm). An interpenetrating Ni network was well developed as can be seen in the lower right-hand side of Fig. 10 after reduction. Looking at the electrolyte interface, tiny nickel particles of less than 0.5 μm in size were embedded individually as inclusions. At the opposite side, the interface to the Ni/TiO_2 substrate, the nickel grains were considerably coarser with a size of up to 3 μm. Note that the electrical contact between anode and the nickel network of the substrate is provided through these larger sized nickel grains.

With increasing sintering temperature the anode became less porous and both zirconia and nickel grains tend to agglomerate accompanied by an increase in grain size. Within the anode the agglomeration of nickel caused a reduction in contiguity of the interpenetrating nickel network. At the interface anode/substrate the size of the nickel grains increased to 4 μm and appeared to be larger than within the substrate. From the observations, it is concluded that the maximum triple phase boundary length of nickel, zirconia and porosity can only be achieved when the co-firing temperature is below the partial melting temperature of 1300°C. The reason is that partial melting at the anode/substrate interface occurred at temperatures higher than 1300°C, which caused the anode to densify considerably more strongly resulting in a reduced porosity and increased zirconia grain size. The agglomeration of nickel and the accompanying degradation of the nickel network reduces the amount of triple phase boundaries, which is particularly detrimental to cell performance. These considerations lead to the conclusions that with the aim of good cell performance co-firing should be carried out in the temperature regime between 1280°C and 1300°C.

3.6. Thermoelastic bending behavior during assembly cycles

For the stack assembly process it is interesting to know the bending behavior of individual $NiO/NiTiO_3$-SAE

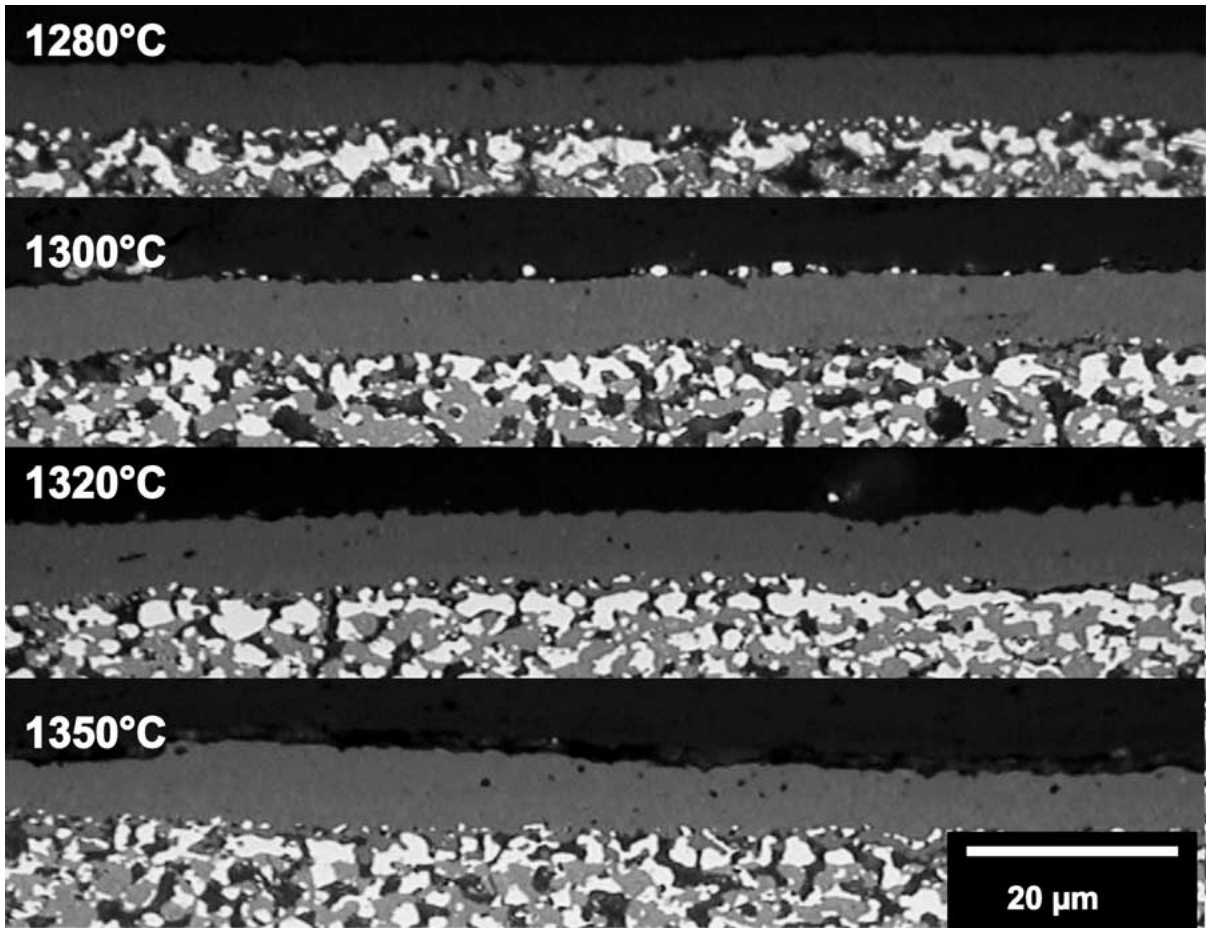

Figure 9 Electrolyte layer (dark gray) on top of anode and Ni/TiO_2 substrates after co-firing at 1280°C (195 min), 1300°C (120 min), 1320°C (75 min) and 1350°C (30 min) and reduction at 900°C (2 h).

assemblies during temperature changes between room temperature and 900°C in reducing gas atmosphere as shown in Fig. 11. From the diagram it is apparent that the central deflection was constantly zero from room temperature up to 700°C, i.e. in this temperature range the sample remained planar. This proves that the adjustment of the thermal expansion coefficients (TEC) of oxidized substrate and electrolyte was successful. In fact, the TEC values of the NiO/$NiTiO_3$ substrate and Ni/TiO_2 cermet are very similar as shown by the theoretical values of 11.3 and $11.5 \times 10^{-6}\,K^{-1}$, respectively, and the experimental values in Figs 1 and 2 of 11.1 and $11.6 \times 10^{-6}\,K^{-1}$, respectively. At 750°C, however, strong bending started towards the substrate side. The deformation rate rapidly increased with increasing temperature and was highest at 800°C. After heating to the final temperature of 900°C and a 45-min hold no further bending occurred. The maximum deflection increase corresponded to 3.2 mm for a specimen length of 100 mm. The bending above 700°C is entirely related to the reduction of NiO to Ni within the substrate and the accompanying loss of mechanical strength. It was not observed during heating in air. This loss of mechanical strength, which was already observed during thermal expansion measurements [14], can be expected especially in the sample co-fired at 1400°C as the NiO forms a continuous coating around the $NiTiO_3$ particles (Fig. 4). Bending occurred due to the stress relaxation within the electrolyte layer arising from the co-firing step. Note that reduction of NiO to Ni already becomes reasonably fast at 650°C [19], but the heating rate used here caused a delay.

Of course, the maximum curvature was achieved when the reduction of the NiO phase was completed, i.e. after 45 min at 900°C. It can be speculated that reduction-related bending will be substantially reduced in those assemblies which were co-fired at lower temperatures, especially at 1280°C. In this case a stiff and non-deforming ceramic network of TiO_2 grains will avoid the shrinkage of the Ni-interpenetrating network. As a consequence, the volume decrease of NiO will be compensated mainly by pore formation. A smaller bending may result due to higher substrate elasticity in combination with increased porosity.

The advantage over membrane-electrode assemblies (MEAs) based on the standard Ni/8YSZ substrate is enormous. Titania-based MEAs are planar after co-firing and are therefore easy to assemble within a stack. Better electrical contact is achieved with lower assembly pressure and is kept constant during heating to sealing temperature. Thermal cycling will not introduce stresses due to thermoelastic bending and there is no danger of losing electrical contact. Note that the softening of the Ni/TiO_2 cermet at temperatures above 800°C [14] represents another advantage since it enables improved relaxation of stresses introduced by stack manufacturing. However, no long-term tests have been conducted so far and therefore there is no

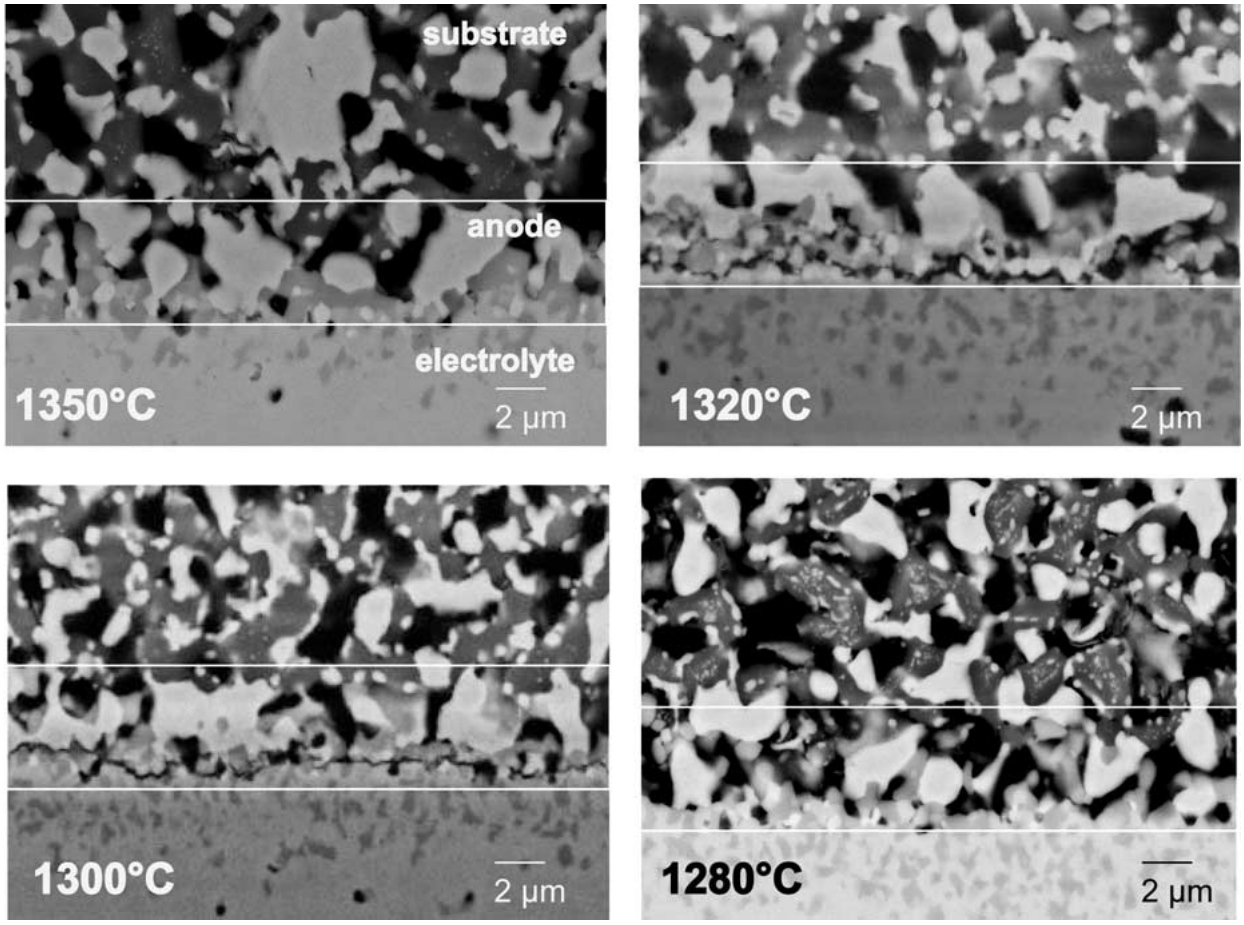

Figure 10 SEM micrographs showing the anode of Ni/TiO_2-SAE assemblies sintered at 1280°C (195 min), 1300°C (120 min), 1320°C (75 min) and 1350°C (30 min) and subsequently reduced at 900°C (2 h). The Ni/8YSZ-based anode is located between the given lines.

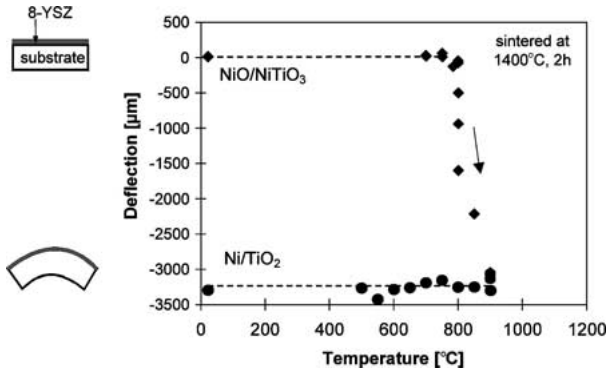

Figure 11 Thermoelastic bending behavior of a $NiO/NiTiO_3$-SAE assembly before and after reduction to Ni/TiO_2. The TECs of the assembly are well adjusted so that thermoelastic bending is negligible. Strong bending beyond 700°C results from decreased mechanical strength of the substrate due to reduction of NiO to Ni.

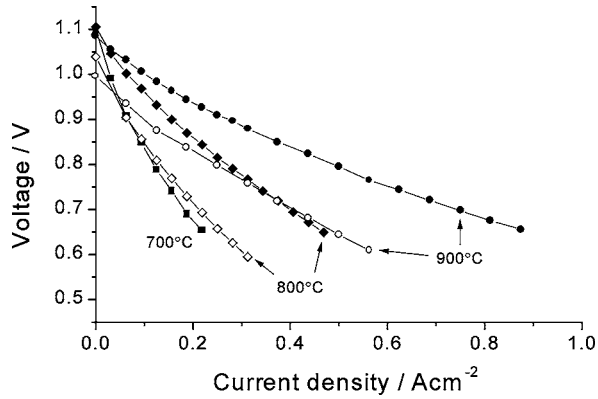

Figure 12 Current-voltage characteristics of an SOFC with $NiO/NiTiO_3$-SAE assembly (open symbols) and for comparison a conventional SOFC with Ni/8YSZ substrate (solid symbols) at 700, 800 and 900°C.

experience concerning long-term mechanical stability and long-term seal performance.

3.7. Electrochemical performance

The Ni/TiO_2-SAE assembly sintered at 1350°C delivered a slightly increasing voltage from 0.73 to 0.75 V during the constant load period of 144 h at 150 mA/cm^2 and at 800°C. The current-voltage curves revealed that at 700 mV a current density of 130 mA/cm^2 was obtained at 750°C and 400 mA/cm^2 at 900°C. This corresponds to a power output of 0.09 W/cm^2 and 0.28 W/cm^2, respectively. For comparison the current-voltage curves of a conventional SOFC with Ni/8YSZ substrate and identical cathode are shown in Fig. 12. As can be seen here, the power output obtained for the cell with the Ni/TiO_2 substrate was approx. half that of the standard cell. Therefore a similar current-voltage curve of the cell with the Ni/TiO_2 substrate is achieved at about 100°C higher temperatures as for the standard cell. Furthermore, it is worth mentioning that the open circuit voltage (OCV) was significantly lower compared with the OCV of the standard cell indicating

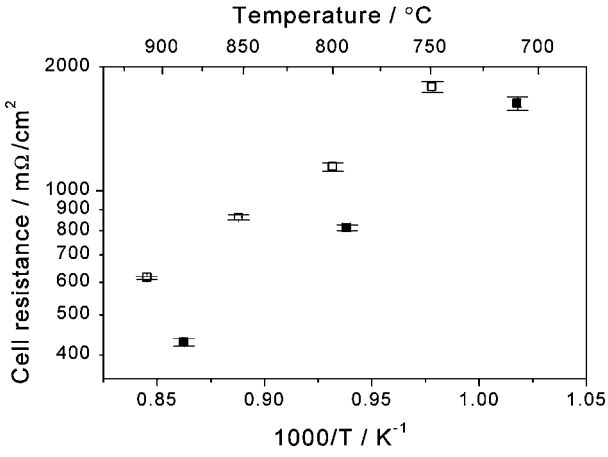

Figure 13 Temperature dependence of the cell resistance of the SOFC with Ni/TiO_2 substrate (□) and of the SOFC with Ni/8YSZ substrate (■) determined from the slopes of the current-voltage curves as shown in Fig. 12.

an imperfect gastightness of the electrolyte layer and therefore nonoptimized co-firing conditions.

From the cell resistance, which was determined from the current-voltage curves as the slope in the linear region of the curves at high current densities and which ranged from about 600 to 1800 $m\Omega \cdot cm^2$ (Fig. 13) for temperatures of 900 and 750°C, respectively, an activation energy 65.5 ± 3.7 kJ/mol was determined. The cell with the Ni/8YSZ substrate revealed a significantly lower cell resistance (at 800°C about 250 $m\Omega\ cm^2$), but a very similar slope leading to an activation energy of 70.2 ± 0.6 kJ/mol.

Only a limited number of experiments have been conducted so far with respect to the electrochemical performance of cells with titania-based substrates. A number of data are still lacking for a proper evaluation, especially those regarding reproducibility and long-term stability. However, from the experiments which were exclusively run on the cell co-fired at 1350°C some important conclusions can be drawn. The activation energy of the cell is similar to that of the standard cells at FZJ with Ni/8YSZ-based substrates (Fig. 13). This indicates that the mechanisms controlling the electrochemical performance are the same. Assuming this, the differences in cell performance then result from differences in electrochemically active surface. Due to the relatively high co-firing temperature applied the anode exhibited a comparatively small triple phase boundary length and agglomeration of the Ni particles at the substrate/anode interface (Fig. 10). As a consequence, the cell performance was expected to be lower than that of standard cells and the cell resistance is increased. Increasing the triple phase boundary by reducing the co-firing temperature should result in an improved cell performance. Related experiments on this topic are currently under way.

4. Conclusions

Anode substrates based on NiO and TiO_2 were fabricated matching the TEC of the 8YSZ electrolyte. With the appropriate sintering conditions the microstructure can be tailored such that gas permeability is improved by a factor of three compared to standard substrates with the same porosity. Electrical conductivity can be tripled with respect to standard substrates with equal gas permeability due to the highly interconnecting metal phase network.

Co-firing the substrates with an anode and electrolyte coating is a reliable way of achieving MEAs with dense electrolyte. With the temperature and the time of the co-firing cycle the amount of triple phase boundaries in the anode and the planarity of the substrate can be controlled. MEAs using the newly developed TiO_2-based substrates do not bend during temperature changes, neither in the oxidized nor in the reduced state due to well adjusted TEC. Bending upon reduction is not necessarily a critical point as the cells are constrained and pressed in the stack while stress relaxation is expected due to the softening of the reduced specimens investigated. This will improve stack assembly, electrical contact and sealing during thermal cycling of stacks.

Electrochemical performance is lower than for conventional cells with Ni/8YSZ substrates, but the critical issues leading to performance loss have been identified and can be solved with improved co-firing conditions.

Acknowledgements

The authors thank W. Fischer (SEM/EDX), R. Fisseler (ceramography), D. Simwonis (gas permeability and electrical conductivity measurements), and I. C. Vinke (electrochemical tests) for their experimental contributions to this work.

References

1. H. P. BUCHKREMER, U. DIEKMANN, L. G. J. DE HAART, H. KABS, U. STIMMING and D. STÖVER, in Proceedings of the 5th Int. Symp. Solid Oxide Fuel Cells (SOFC-V), edited by U. Stimming, S. C. Singhal, H. Tagawa and W. Lehnert (The Electrochemical Society, Pennington, NJ, 1997) p. 160.
2. H. ARAI, K. EGUCHI, T. SETOGUCHI, R. YAMAGUCHI, K. HASHIMOTO and H. YOSHIMURA, in Proceedings of the 2nd Int. Symp. SOFC (SOFC-II), Athens, edited by F. Grosz, P. Zegers, S. C. Singhal and O. Yamamoto (Commission of the European Communities, Brussels, 1991) p. 167.
3. H. P. BUCHKREMER, U. DIEKMANN and D. STÖVER, in Proceedings of the 2nd Eur. SOFC Forum, Oslo, edited by B. Thorstensen (The European Solid Oxide Fuel Cell Forum, Oberrohrdorf, Switzerland, 1996) p. 221.
4. D. STOLTEN, R. SPÄH and R. SCHAMM, in Proceedings of the 5th Int. Symp. Solid Oxide Fuel Cells (SOFC-V), edited by U. Stimming, S. C. Singhal, H. Tagawa and W. Lehnert (The Electrochemical Society, Pennington, NJ, 1997) p. 88.
5. R. WILKENHÖNER, W. MALLÉNER, H.-P. BUCHKREMER, TH. HAUBER and U. STIMMING, in Proceedings of the 2nd Eur. SOFC Forum, Oslo, Vol. 2, edited by B. Thorstensen (The European Solid Oxide Fuel Cell Forum, Oberrohrdorf, Switzerland, 1996) p. 279.
6. M. BROWN, S. PRIMDAHL, M. MOGENSEN and N. M. SAMMES, *J. Australasian Ceram. Soc.* **34** (1998) 248.
7. F. TIETZ, F. J. DIAS and A. NAOUMIDIS, in Proceedings of the 3rd European Solid Oxide Fuel Cell Forum, Vol. 1, edited by P. Stevens (The European Solid Oxide Fuel Cell Forum, Oberrohrdorf, Switzerland, 1998) p. 171.
8. R. W. STEINBRECH, A. CARON, G. BLAß and F. J. DIAS, in Proceedings of the 5th Int. Symp. Solid Oxide Fuel Cells (SOFC-V), edited by U. Stimming, S. C. Singhal, H. Tagawa and

W. Lehnert (The Electrochemical Society, Pennington, NJ, 1997) p. 727.
9. F. MESCHKE and R.W. STEINBRECH, in Proceedings of the 6th Int. Symp. Solid Oxide Fuel Cells (SOFC-VI), edited by M. Dokiya and S. C. Singhal (The Electrochemical Society, Pennington, NJ, 1999) p. 1047.
10. J. P. THOMAS, *J. Appl. Phys.* **41** (1970) 5104.
11. Y. S. TOULOUKIAN, R. K. KIRBY, R. E. TAYLOR and T. Y. R. LEE, in "Thermophysical Properties of Matter," Vol. 13: Thermal Expansion—Nonmetallic Solids (IFI/Plenum, New York, 1977).
12. R. MAENNER, E. IVERS-TIFFÉE, W. WERSING and W. KLEINLEIN, in Proceedings of the 2nd Eur. Ceram. Soc. Conf. (Euro-Ceramics II), edited by G. Ziegler and H. Hausner (Deutsche Keramische Gesellschaft, 1991) p. 2085.
13. F. TIETZ, G. STOCHNIOL and A. NAOUMIDIS, in Proceedings of the 5th Eur. Conf. on Advanced Materials, Processes and Applications (Euromat '97), Vol. 2, edited by L. A. J. L. Sarton and H. B. Zeedijk (Netherlands Society for Materials Science, 1997) p. 271.
14. F. TIETZ, F. J. DIAS, B. DUBIEL and H. J. PENKALLA, *Mater. Sci. Eng. B* **B68** (1999) 35.
15. D. SIMWONIS, A. NAOUMIDIS, F. J. DIAS, J. LINKE and A. MOROPOULOU, *J. Mater. Res.* **12** (1997) 1508.
16. D. SIMWONIS, F. J. DIAS, A. NAOUMIDIS and D. STÖVER, in Proceedings of the 5th Eur. Conf. on Advanced Materials, Processes and Applications (Euromat '97), Vol. 2, edited by L. A. J. L. Sarton and H. B. Zeedijk (Netherlands Society for Materials Science, 1997) p. 375.
17. R. FÖRTHMANN, G. BLASS and H.-P. BUCHKREMER, in Proceedings of the 5th Int. Symp. Solid Oxide Fuel Cells (SOFC-V), edited by U. Stimming, S. C. Singhal, H. Tagawa and W. Lehnert (The Electrochemical Society, Pennington, NJ, 1997) p. 1003.
18. F. TIETZ, in Proceedings of the 9th CIMTEC—World Ceramic Congress and Forum on New Materials, Vol. 24: Innovative Materials in Advanced Energy Technologies, edited by P. Vincenzini (Techna Publishers S.r.l., Faenza, Italy, 1999) p. 61.
19. D. SIMWONIS, G. STATHIS, F. TIETZ, R. W. STEINBRECH and A. NAOUMIDIS, Proceedings of the 3rd European Solid Oxide Fuel Cell Forum, Vol. 2, edited by P. Stevens (The European Solid Oxide Fuel Cell Forum, Oberrohrdorf, Switzerland, 1998) p. 219.
20. W. LAQUA, E. W. SCHULZ and B. REUTER, *Z. Anorg. Allg. Chem.* **433** (1977) 167.
21. R. VAßEN, R. W. STEINBRECH, F. TIETZ and D. STÖVER, Proceedings of the 3rd European Solid Oxide Fuel Cell Forum, Vol. 1, edited by P. Stevens (The European Solid Oxide Fuel Cell Forum, Oberrohrdorf, Switzerland, 1998) p. 557.

Received 20 April 2000
and accepted 9 July 2001